



ISTITUTO NAZIONALE DI RICERCA METROLOGICA Repository Istituzionale

Enhanced selective sonosensitizing efficacy of ultrasound-based anticancer treatment by targeted gold nanoparticles

This is the author's submitted version of the contribution published as:

Original

Enhanced selective sonosensitizing efficacy of ultrasound-based anticancer treatment by targeted gold nanoparticles / Brazzale, Chiara; Canaparo, Roberto; Racca, Luisa; Foglietta, Federica; Durando, Giovanni; Fantozzi, Roberto; Caliceti, Paolo; Salmaso, Stefano; Serpe, Loredana. - In: NANOMEDICINE. - ISSN 1743-5889. - 11:23(2016), pp. 3053-3070-3070. [10.2217/nnm-2016-0293]

Availability:

This version is available at: 11696/54592 since: 2021-03-06T09:30:56Z

Publisher:

Future Medicine Ltd

Published

DOI:10.2217/nnm-2016-0293

Terms of use:

This article is made available under terms and conditions as specified in the corresponding bibliographic description in the repository

Publisher copyright

(Article begins on next page)

Enhanced selective sonosensitizing efficacy of ultrasound-based anticancer treatment by targeted gold nanoparticles

Chiara Brazzale¹, Roberto Canaparo^{2*}, Luisa Racca², Federica Foglietta², Gianni Durando³, Roberto Fantozzi², Paolo Caliceti¹, Stefano Salmaso^{1*}, Loredana Serpe²

¹Department of Pharmaceutical and Pharmacological Sciences, University of Padova, Via F. Marzolo 5, 35131 Padova, Italy

²Department of Drug Science and Technology, University of Torino, Via P. Giuria 13, 10125 Torino, Italy

³National Institute of Metrological Research (INRIM), Strada delle Cacce 91, 10135 Torino, Italy

***Co-corresponding Authors:**

Roberto Canaparo, PhD

Department of Drug Science and Technology, University of Torino

Via Pietro Giuria 13, 10125 Torino, Italy

Tel: +390116706235 Fax: +390116706230 e-mail: roberto.canaparo@unito.it

Stefano Salmaso, PhD

Department of Pharmaceutical and Pharmacological Sciences, University of Padova

Via F. Marzolo 5, 35131 Padova, Italy

Tel: +390498271602 Fax: +390498275366 e-mail: stefano.salmaso@unipd.it

ABSTRACT

Aim: This study investigates cancer targeted gold nanoparticles as ultrasound sensitizers for the treatment of cancer. **Methods:** The ultrasound sensitizer activity of folate-PEG decorated gold nanoparticles (FA-PEG-GNP) have been studied on human cancer cell lines that over-express folate receptors (KB and HCT-116) and another that does not (MCF7), at two ultrasound energy densities ($8 \times 10^{-6} \text{ J cm}^{-2}$ and $8 \times 10^{-5} \text{ J cm}^{-2}$, for 5 min at 1.866 MHz). **Results:** FA-PEG-GNP selectively targeted KB and HCT-116 cells and a remarkable reduction in cancer cell growth was observed upon ultrasound exposure, along with significant reactive oxygen species generation and increase in necrotic cells. **Conclusion:** The combined use of targeting capacity and the ultrasound sensitizing effect, make FA-PEG-GNP promising candidates for the site-specific cancer treatment.

KEYWORDS

Gold nanoparticles; cancer targeting; sonosensitizer; nanosonosensitizer; therapeutic ultrasound; sonodynamic treatment; cancer.

INTRODUCTION

Ultrasound (US) can affect the functional and structural properties of biological tissues via a number of mechanisms, generally classified as thermal or non-thermal, which are dependent on factors such as frequency, pressure, power and exposure time [1, 2]. The effects of US can be exploited for therapeutic purposes. The thermal anti-cancer applications of US, such as high intensity focused ultrasound (HIFU) which induces coagulative necrosis at a precise focal point [3], have been more extensively studied than the therapeutic uses of the non-thermal US effects. The effects of US on tissue include, other than the direct thermal effect: i) alteration of biobarrier permeability ii) drug delivery iii) sonodynamic activity [1]. The last effect has recently been the driving force behind a great deal of interest, as the peculiar phenomenon of cavitation is opening new perspectives for cancer treatment [4]. US-induced inertial cavitation generates gas bubbles that grow to near resonance size and expand to a maximum before collapsing violently with the conversion of the diffused energy into highly localized heat and pressure. Bulk temperature and pressure within the imploding cavities can reach values of up to 10,000 °K and 800 atm, respectively. These extreme conditions can induce a variety of physical events both within and around the bubble, including an increase in energy density that can generate light: a phenomenon known as sonoluminescence [5, 6]. Furthermore, US-induced inertial cavitation can transfer energy to surrounding molecules and alter their chemical properties, yielding sonosensitizers and finally cancer cell death. Therefore, the combination of US-induced inertial cavitation and sonosensitizing agent has been defined sonodynamic therapy (SDT) [7, 8].

Although the SDT mechanism is still a matter of much debate, it is generally accepted that the main effectors of sonosensitized cell damage are short-lived chemical species, namely ROS and free radicals, generated as a consequence of the selective accumulation of the sonosensitizing agent in tumors and triggered by US-induced acoustic cavitation [9]. Therefore, SDT can be exploited as a “remotely controlled” bimodal therapeutic treatment, in which, a non-toxic molecule or system (chemical actuator), i.e. the sonosensitizer, is activated by US (physical activator) yielding oxidative

damage and consequent cancer cell death.

SDT is thus achieved by an external physical stimulus that activate molecules or colloidal systems yielding, in turn, a biological effect only when the former and the latter are combined together. Accordingly, SDT has similar potential to photodynamic therapy (PDT), a clinically approved bimodal anticancer approach, where light is used to activate particular chemical compounds, i.e. photosensitizers, to kill cancer cells. Nevertheless, PDT has some drawbacks, the most important of which being the poor diffusion of light through human tissues, even at long wavelengths in the NIR. This limits PDT's application to superficial tumor treatment [10]. As US easily propagates through the body, allowing the targeting of more deeply-seated cancer lesions without the need for invasive devices, STD can be a promising approach to overcome this drawback [4].

Although SDT appears to be an encouraging new approach for cancer therapy, significant progresses in the field will depend on the development of US specific sonosensitizers that can efficiently convert US-induced cavitation into ROS production within the tumor tissue in a US-dose dependent manner.

Gold nanoparticles (GNP) have been brought to the forefront of cancer research in recent years because they are easily produced and can support great versatility in their surface coatings. Furthermore, GNP posses tunable optical and thermal properties as well as high biocompatibility that make them suitable systems for clinical application [11-13]. Moreover, the GNP plasmonic effect that derives from surface plasmon resonance (SPR), a unique photophysical response to light in which the oscillating electromagnetic field of light induces a collective coherent oscillation of free electrons (conduction band electrons) in a metal, distinguishes them from other nanosystems [14]. This SPR effect, which results from photon confinement to a small particle size, is also correlated to some nanoparticle properties including their radiative, absorption and scattering, and non-radiative, the quick conversion of strongly absorbed light to heat, properties [15]. Since GNP absorb light millions of times more intensely than organic dyes [14], they have already been proposed for photothermal therapy (PTT), a treatment for shallow cancer (e.g. skin cancer) in which

photon energy is converted to heat in order to induce cellular damage via hyperthermic effects [16]. Their good uptake by mammalian cells, their low toxicity, their peculiar interaction with light (i.e. SPR) and the sonoluminescence hypothesis underlining STD, all make GNP ideal candidates for use as sonosensitizing agents in SDT and also provide the drive for a step forward for clinical applications in this field.

We have developed folic acid conjugated gold nanoparticles (FA-PEG-GNP) in order to further improve the site-specificity of the sonodynamic treatment of cancer. The enhanced specificity and intracellular access of these systems has led to the active targeting of colloidal therapeutic systems attracting considerable interest [12, 17, 18]. Folic acid (FA), a low molecular weight vitamin, is a typical cell-targeting agent in virtue of its binding affinity toward the folate receptor (FR) that is known to be over-expressed by a variety of human cancer cells. Moreover, the FR distribution appears to rise as cancer progress, whereas FR is only minimally distributed in normal cells [19, 20].

This work aims to provide a proof-of-concept study for the use of targeted gold nanoparticles as site-selective sonosensitizers for ultrasound triggered cancer cell death since, to the best of our knowledge, such an attempt has not yet been reported.

MATERIALS AND METHODS

Materials

Dicyclohexylcarbodiimide (DCC), N-hydroxysuccinimide (NHS), triethylamine, folic acid, 5,50-dithio-bis(2-nitrobenzoic acid) (DTNB), Tris(2-carboxyethyl)phosphine hydrochloride, sodium citrate dihydrate and tetrachloroauric(III) acid, fetal bovine serum, RPMI 1640, McCoy's 5A, FFDMEM, glutamine solution, penicillin-streptomycin solution, glucose solution and trypsin-EDTA solution were all purchased from Sigma (St. Louis MO, USA). The sephadex G25 superfine resin was obtained from Pharmacia Biotech AB (Uppsala, Sweden). mPEG_{2kDa}-SH and NH₂-PEG_{3.5kDa}-SH were purchased from Iris Biotech GmbH (Marktredwitz, Germany). Spectra/Por Float-a-lyzer G2 (MW cutoff = 0.5-1 kDa) was obtained from SpectrumLabs (Rancho Dominguez, CA).

Synthesis of folate-PEG_{3.5 kDa}-SH

Folic acid (50.0 mg, 0.113 mmol) was dissolved in 1 mL of anhydrous DMSO. NHS (15.6 mg, 0.136 mmol) followed by DCC (28.1 mg, 0.136 mmol) were added to the solution. The mixture was stirred overnight in the dark and then filtered to remove the insoluble dicyclohexylurea. N-hydroxysuccinimidyl-ester-activated folic acid was isolated by precipitation in cold diethyl ether. The precipitate was washed several times with cold diethyl ether. The NHS ester activated folic acid was then dried under reduced pressure. NHS-folic acid (25 mg, 0.046 mmol) and NH₂-PEG_{3.5 kDa}-SH (54.1 mg, 0.015 mmol) were dissolved in 1 mL of anhydrous DMSO, with the addition of triethylamine (2.1 μ L, 0.015 mmol). The reaction mixture was stirred for 12 h at room temperature in the dark and then added dropwise to diethyl ether (40 mL). The precipitate was recovered by centrifugation and dried under *vacuo*. The crude product was purified from the unreacted folic acid using size exclusion chromatography and a Sephadex G-25 resin eluted with an aqueous ammonia solution (pH 9). The column fractions were tested using UV-Vis spectroscopy at 363 nm and the iodine test [21] to assess folate and PEG, respectively. The fractions that were positive in both

assays were collected and freeze-dried. The yellow powder was treated by reduction in order to regenerate free thiol groups. The material (20 mg, corresponding to 8.2 μ moles of FA-PEG_{3.5kDa}-SH) and TCEP (20.5 mg, 82 μ moles) were dissolved in 50 mM acetate buffer at pH 5 and left under stirring for 3 h. The mixture was then dialysed using a Spectra/Por Float-a-lyzer G2 (MW cutoff = 0.5-1 kDa) with a 1 mM HCl, 1 mM EDTA solution as the releasing medium. The dialysis was performed for 2 days and then the FA-PEG_{3.5kDa}-SH solution was then freeze-dried.

The lyophilized FA-PEG_{3.5kDa}-SH was dissolved in PBS pH 7.4 and analyzed using UV-Vis spectroscopy at 363 nm (molar extinction coefficient of folate at 363 nm in PBS, pH 7.4 is 6.197 M⁻¹ cm⁻¹ [22]) and iodine test to assess the conjugation efficiency, and using the Ellman's assay [23] to determine the percentage of free thiol groups. FA-PEG_{3.5 kDa}-SH was characterized using MALDI mass spectroscopy on a 400 Plus MALDI TOF/TOF Analyzer (AB Sciex, Framingham, MA, USA).

Product purity was evaluated using reverse phase chromatographic analysis on a Jasco HPLC system (Tokio, Japan), equipped with two PU-2080 Plus pumps, a UV-2075 Plus detector (set at 363 nm), an analytic column Luna (C18, 5 μ , 300 Å, 250 x 4.6 mm) from Phenomenex (Torrance, CA, U.S.A.) and eluted in gradient mode with 10 mM ammonium acetate buffer, pH 6.5 (eluent A) and acetonitrile (eluent B). Eluent B was increased linearly from 10 to 40% over 40 min.

¹H NMR (300 MHz, DMSO-*d*₆): δ 8.64 (s, C7-H of FA, 1H), 7.64 (d, 2',6'-H of FA, 2H), 6.65 (d, 3',5'-H of FA, 2H), 4.35-4.26 (m, α -CH of Glu of FA, 1H), 3.50 (s, PEG, ~316H), 2.89 (t, CH₂-S, 2H).

Gold nanoparticle preparation

The preparation of gold nanoparticles was performed according to the Turkevich method [24] using sodium citrate as the reducing and capping agent. Glassware was extensively washed with aqua regia (3:1 v/v of 12.2 M Hydrochloric acid / 14.6 M Nitric acid) and then rinsed with deionized water. A 0.25 mM tetrachloroauric solution was prepared in Milli-Q water (100 mL) and heated up

to 75 °C under stirring. Trisodium citrate dihydrate (100 mg) was dissolved in Milli-Q water and 3 mL of the solution (0.34 M) was added dropwise to the HAuCl₄ solution. The mixture was left under stirring for 1 h. Then, the gold colloidal suspension was cooled to room temperature and extensively characterized.

A 18 µL volume of a 0.5 mg/mL FA-PEG_{3.5kDa}-SH aqueous solution was mixed with 9 µL of a 50 µg/mL mPEG_{2kDa}-SH aqueous solution. The polymer mixture was immediately added to 15 mL of a 3 nM gold nanoparticle suspension to a final 50:5:1 FA-PEG_{3.5kDa}-SH / mPEG_{2kDa}-SH / GNP molar ratio. The suspension was left under rotational stirring overnight at room temperature. Then the mixture was centrifuged at 14,000 rpm for 30 minutes at 4 °C to isolate the particles and the supernatant was lyophilized and redissolved in 150 µL of Milli-Q water and analysed by UV-Vis spectroscopy at 363 nm and 535 nm (Iodine test) to assess the quantity of unbound FA-PEG_{3.5 kDa} -SH and mPEG_{2 kDa}-SH.

The particle pellet was washed three times with Milli-Q water and resuspended in 15 mL of Milli-Q water. The particle suspension was then added of 72 µL of 5 mg/mL mPEG_{2kDa}-SH aqueous solution in order to extensively decorate the particle surface with the thiolated methoxy-PEG-SH (mPEG_{2 kDa}-SH/GNP molar ratio= 4000:1). The mixture was left overnight under rotational stirring. The resulting suspension of folate coated PEGylated gold nanoparticles (FA-PEG-GNP) was centrifuged at 14,000 rpm for 30 minutes at 4 °C. The FA-PEG-GNP pellet was isolated from the supernatant, which was subsequently analyzed using the Iodine test to assess the quantity of unbound PEG.

Control non-targeted particles (mPEG-GNP) were produced as described above using mPEG_{3.5kDa} –SH instead of FA-PEG_{3.5kDa} -SH.

Gold nanoparticle characterization

DLS analysis. The size of naked and functionalized GNP was measured at 25 °C using dynamic light scattering (DLS) on a Zetasizer NanoZS (Malvern Instruments Ltd, UK) equipped with a red

laser (633 nm) at a fixed angle of 173°. “DTS applications 6.12” software was used to analyse the data. All sizes reported were based on number average.

TEM analysis. Transmission electron microscopic (TEM) imaging was performed on a Tecnai G2 microscope (FEI *Tecnai*, Oregon, USA). Ten μL of naked particle suspension (1 nM) in milli-Q water was placed on a carbon coated copper grid and the water was allowed to dry at room temperature. The average particle size was calculated from the average of 100-300 individual particle diameters using “SIS Soft Imaging GmbH” image analysis software. The targeted particles (FA-PEG-GNP) and control PEGylated particles (mPEG-GNP) were negatively stained with 1% uranyl acetate dissolved in distilled water and analysed according to the same protocol.

Concentration assessment. The concentrations of gold nanoparticle suspensions were assessed according to the method reported by Liu et al. [25]. Equation (1) was applied to derive the particle molar extinction coefficient, which referred to absorbance at 506 nm (ϵ_{506}):

$$(1) \quad \ln \epsilon = k \ln D + a$$

where D is the diameter of the nanoparticles (obtained from DLS analysis), k and a are two constants whose values are 3.32111 and 10.80505 respectively [26, 27]. ϵ_{506} was then used to calculate the particle concentration according to the Lambert–Beer law.

Cell culture

Human MCF7 breast adenocarcinoma (ICLC, Interlab Cell Line Collection, Genova, Italy), HCT-116 colon carcinoma (ICLC) and KB epidermoid carcinoma (ECACC, European Collection of Cell Culture, Salisbury, UK) cell lines were cultured as monolayer in RPMI 1640, McCoy’s 5A and folate free DMEM (FFDMEM) growth medium, respectively, supplemented with 10% fetal bovine serum (v/v), 2.0 mM L-glutamine, 100.0 UI/mL penicillin and 100.0 $\mu\text{g/mL}$ streptomycin in a humidified atmosphere containing 5% CO_2 at 37 °C. Cells were detached using 0.05% trypsin-0.02% EDTA solution (Sigma), suspended in culture medium and seeded at the appropriate cell concentrations for cell culture experiments.

Cell folate receptor expression

In order to assess folate receptor expression on cell lines, 1.0×10^3 MCF7, 0.4×10^3 HCT-116, 0.7×10^3 KB cells were cultured in 6-well culture plates (Techno Plastic Products, Trasadingen, Switzerland) in 2 mL of respective culture medium. After 72 h cells were incubated with 10 $\mu\text{g/mL}$ folate receptor α monoclonal antibody (Enzo Life Science, New York, USA) for 2 h at 37 °C. Cells were then washed with phosphate-buffered saline (PBS, pH 7.4, 150 mM) and incubated with 0.5 $\mu\text{L/mL}$ rabbit F(ab')₂ polyclonal secondary antibody-Alexa Fluor[®] 488 (Abcam, Cambridge, UK) for 1 h at 37 °C [28]. Finally, cells were trypsinized, normalized to 5.0×10^5 cells in 0.3 mL of PBS and analyzed on a C6 flow cytometer (Accuri Cytometers, Inc. Ann Arbor, MI USA) and a total of 10,000 events were recorded. Results were expressed as integrated mean fluorescence intensity (iMFI), defined as the percentage of FR-positive cells multiplied by the mean fluorescence intensity of FR-positive cells.

Cell uptake studies

MCF7, HCT-116 and KB cells were seeded in 12-well plates (500 μL per well, 1×10^6 cells/mL) and grown for 24 h. The medium was removed, cells washed twice with PBS and either 1 nM FA-PEG-GNP or control non-targeted mPEG-GNP suspensions in FFD MEM were added (1 mL/well). After 2 h of incubation at 37 °C, the particle containing media were removed and the cells were washed 3 times with PBS without MgCl_2 and CaCl_2 . The cells were then detached using 1% w/v trypsin treatment (150 μL /well). Trypsin was quenched by adding 500 μL of PBS containing MgCl_2 and CaCl_2 to each well and cells were recovered by centrifugation at 1,000 rpm for 5 minutes. The cell pellets were washed twice with PBS and then a 0.1 w/v% Triton[®] X-100 solution in water (600 μL) was added and exposed to sonication for 1 h. The samples were then centrifuged at 1,000 rpm for 5 minutes and number of cells per sample was assessed on 100 μL of the cell lysate using the BCA Protein Assay Kit (Thermo Fisher Scientific Inc., Waltham, MA-USA). Five hundred μL of cell lysate were digested by aqua regia treatment (5 mL) at 80 °C for 1 h to dissolve gold. The

mineralized lysates were suitably diluted with 0.32 M HCl and analyzed by Atomic Absorption Spectroscopy (AAS) to assess gold concentration on a Varian AA240 Zeeman instrument equipped with a GTA120 graphite furnace, a Zeeman background corrector and an autosampler (Varian Inc., Palo Alto, CA-USA). Nanoparticles number per cell was derived from gold concentration and the number of cells in the samples.

Cell uptake inhibition assay. MCF7, HCT-116 and KB cells seeded in 12-well plates were washed twice with PBS and incubated with 1 nM FA-PEG-GNP or 1 nM mPEG-GNP suspensions in FFDMEM medium supplemented with free folic acid (200 μ M). After an incubation time of 2 h at 37 °C, the cell samples were processed as mentioned above for gold quantification by atomic absorption analysis.

Transmission electron microscopy (TEM). The intracellular disposition of gold nanoparticles was imaged using TEM analysis. KB cells were seeded at a density of 3×10^5 in 12 well-plates in FFDMEM as reported above. After 24 h, the cells were washed twice with PBS and incubated for 2 h with either a 1 nM FA-PEG-GNP or a mPEG-GNP suspension in FFDMEM medium. The medium was then removed from the wells and the cells were washed three times with PBS and fixed by treatment with 2.5 w/v% glutaraldehyde in 0.1 M sodium cacodylate buffer at 4 °C for 1 h. The cells were washed twice with sodium cacodylate buffer and post fixed in 0.1 M sodium cacodylate buffer containing 1 w/v% osmium tetroxide for 1 h. Each sample underwent a dehydration treatment with ethanol and samples were embedded in fresh EPON resin. Ultrathin sections of the resin embedded samples were cut and imaged on a Tecnai G2 Transmission Electron Microscope (FEI *Tecnai*, Oregon, USA).

Ultrasound treatment

Cells in the exponential growth phase were incubated for 2 h in FFDMEM medium containing either 1 nM of FA-PEG-GNP or the control, non-targeted mPEG-GNP suspension. Cells were then

washed with PBS, trypsinized and normalized to 5.0×10^5 cells in 2.5 mL of PBS in polystyrene tubes for US exposure.

The US field was generated by a plane wave transducer (2.54 cm diameter) in continuous wave, i.e. CW mode, at $f_0 = 1.866$ MHz connected to a power amplifier (Type AR 100A250A; Amplifier Research, Souderton, USA) and a function generator (Type 33250; Agilent, Santa Clara, USA). A mechanical adaptor was built to connect the 1 cm diameter polystyrene tube containing the cells suspended in PBS. When filled with ultrapure water, the adaptor creates highly reproducible measurement conditions at a fixed cell tube distance from the transducer (17 mm) [29].

US exposure was performed for 5 minutes, under a dim light, at two different energy densities: US_n , corresponding to 0.008 mJ/cm^2 energy supplied to the cells which did not cause the temperature of the medium to increase (maximum temperature recorded was 33°C) and US_i , corresponding to 0.080 mJ/cm^2 energy supplied to the cells which increased the temperature of the medium (maximum temperature recorded was 43°C).

Cell proliferation assay

The WST-1 cell proliferation assay (Roche Applied Science, Penzberg, Germany) was used to evaluate the effects of treatment on cell growth. After the various treatments, 2.5×10^3 MCF7, 1.5×10^3 HCT-116 and 2.0×10^3 KB cells were seeded in 100 μl of culture medium in replicates ($n=8$) for each condition in 96-well culture plates (TPP, Trasadingen, Switzerland). MCF7 and HCT-116 cells were incubated for 1.5 h and KB cells for 2 h with WST-1 reagent (10 μl) at 37°C , 24, 48 and 72 h after the US treatment. Well absorbance was measured at 450 and 620 nm (reference wavelength) on a microplate reader (Asys UV340; Biochrom, Cambridge, UK). Cell proliferation data were expressed as a percentage of untreated cells.

Folic acid uptake competition assay. HCT-116 and KB cells were also incubated with FFDMM medium containing 1.0 nM FA-PEG-GNP suspension and 200 μM folic acid (Sigma) for 2 h to evaluate the uptake selectivity of FA-PEG-GNP by cell folate receptor under competition

conditions with folic acid. Cells were then detached and subjected to US treatment as previously described; cell growth was evaluated using a WST-1 assay after 24, 48 and 72 h.

ROS scavenging assay. HCT-116 and KB cells were incubated with the ROS scavenger N-acetylcysteine (NAC; Sigma) in order to evaluate ROS involvement in cell proliferation upon targeted gold nanoparticles incubation and US treatment. Briefly, cells were incubated with 1.0 nM FA-PEG-GNP suspension in FFDMEM medium for 2 h and 5.0 mM NAC was added after 1 h of incubation. Cells were then trypsinized, washed with PBS and exposed to US. Cell growth was assessed using a WST-1 assay after 24, 48 and 72 h.

Cell death analysis

HCT-116 and KB cell death was investigated using the Dead Cell Apoptosis Kit with allophycocyanin (APC)-Annexin V and Sytox[®] Green (Life Technologies, Milan, Italy) with an Accuri C6 flow cytometer. Cells were incubated for 2 h in FFDMEM medium containing 1.0 nM FA-PEG-GNP suspension, cells were then trypsinized, washed with PBS and normalized to 5.0×10^5 cells in 2.5 mL of PBS for US treatment. After US exposure, cells were collected into 3 mL sterile centrifuge tubes for 2 h, washed twice with 1 x Annexin-binding buffer at 1,500 rpm for 5 min and stained with APC-Annexin V and Sytox[®] Green for 15 minutes at 37 °C and samples underwent flow cytometric analyses. Cell debris with low forward light scatter and side light scatter were excluded from the analyses and a total of 10,000 events were analyzed. Fluorescence was collected at 660 and 530 nm to discriminate APC-Annexin V and Sytox[®] Green signals, respectively. Apoptotic and late apoptotic/necrotic cells were discriminated from viable cells using the FCS Express software, version 4 (BD, Bioscience, Milano, Italy).

Intracellular ROS production analyses

Intracellular ROS generation was measured using the 2,7-dichlorodihydrofluorescein diacetate (DCFH-DA; Sigma) probe with a C6 flow cytometer. Briefly, HCT-116 and KB cells were

incubated with a 1.0 nM FA-PEG-GNP suspension in FFDMEM medium for 2 h and 10 μ M DCFH-DA for the last 30 min at 37 °C. Cells were then PBS washed, trypsinized and exposed to US as previously described. ROS production was measured at 1, 5, 15, 30 and 60 min after each treatment and a total of 10,000 events were recorded in the flow cytometric analysis. ROS production was expressed as integrated median fluorescence intensity (iMFI), which was calculated as the product of the frequency of ROS-producing cells and the median fluorescence intensity of the cells. The iMFI ratio was calculated in order to yield the ratiometric increase in fluorescence per time point. The ROS generation in HCT-116 and KB cells treated with FA-PEG-GNP and US was also assessed in the presence of the ROS scavenger, NAC. Briefly, cells were incubated at 37 °C with a 1 nM FA-PEG-GNP suspension in FFDMEM medium for 2 h, then 5.0 mM NAC was added after 1 h of incubation and 10 μ M DCFH-DA after 1.5 h of incubation. Cells were then PBS washed, trypsinized, treated with US and ROS production was assessed using flow cytometric analysis, as previously described.

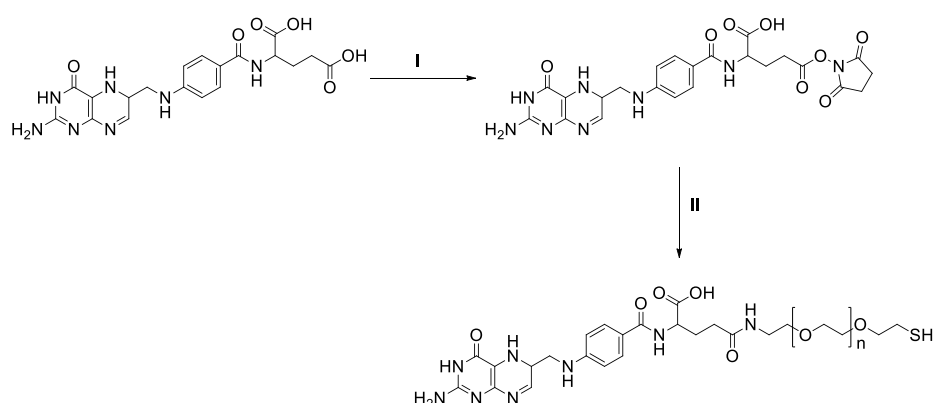
Statistical analysis

Data are shown as the average values \pm standard deviation of three independent experiments. Statistical analyses were performed using Graph-Pad Prism 6.0 software (La Jolla, CA, USA); two-way analysis of variance and Bonferroni's test were used to calculate the threshold of significance. Statistical significance was set at $p < 0.05$.

RESULTS

Synthesis and characterization of folate-PEG_{3.5kDa}-SH (FA-PEG-SH)

Folate-PEG_{3.5kDa}-SH (FA-PEG-SH) conjugate was synthesised according to the method reported in the literature [30] (Scheme I).



Scheme I. Synthesis of FA-PEG-SH: (I) activation of folic acid carboxyl group by NHS and DCC in anhydrous DMSO; (II) conjugation of NHS-ester activated folate to NH₂-PEG_{3.5kDa}-SH in anhydrous DMSO in presence of TEA.

Conjugate was purified from unreacted NHS-folate by gel filtration and then treated with TCEP to reduce the oxidized dimeric species (FA-PEG-S-S-PEG-FA). The TCEP treatment yielded 96 % of -SH groups that were available for the conjugation to the gold nanoparticle surface. Spectrophotometric analyses gave an NH₂-PEG-SH to folic acid conjugation efficiency of 98%. FA-PEG-SH showed MALDI-TOF mass spectrum (Figure 1B) with the typical bell shaped profile for PEG, which was centred at 4000 m/z and was in agreement with the expected molecular weight of the conjugate (Figure 1). This result confirmed that the product contained only the FA-PEG-SH monomer. In fact, no traces of either NH₂-PEG-SH or the dimer (FA-PEG-S-S-PEG-FA) were detected.

The RP-HPLC analysis proved that the purification process yielded efficient removal of the unreacted folic acid, which was in the final product below 0.3 % mol.

Preparation and surface decoration of folate-targeted gold nanoparticles

The gold nanoparticles (GNP) were synthesised by reduction of HAuCl_4 with citrate according to Turkevich's method [31]. Under the conditions selected, a red colloidal 3 nM GNP suspension was obtained. DLS and TEM analyses (Figure 2) showed that the production process yielded dimensionally homogenous particles. DLS analysis showed that the mean size of GNP was 14.6 ± 2.3 nm and the PDI was 0.20 ± 0.08 .

To endow GNP with biorecognition capacity and stealth features, the thiol ending functional polymers, namely the targeting FA-PEG-SH and the mPEG-SH (methoxy-PEG_{2 kDa}-SH), were used for straightforward surface decoration [32]. Targeted GNP were obtained according to a two-step procedure. In the first step, GNP were decorated with FA-PEG-SH by incubation with a 50-fold FA-PEG-SH molar excess with respect to GNP. The particle surface was then saturated with mPEG-SH. Untargeted control particles (mPEG-GNP) were obtained by using only mPEG-SH for the coating.

Spectrophotometric analysis of particle coating efficiency showed that the decoration procedure yielded quantitative conjugation of FA-PEG-SH on the particle surface (98% conjugation efficiency), which corresponds to ~50 units of FA-PEG-SH per particle.

The saturation of the particle surface with 2 kDa mPEG-SH yielded a coating density of 0.92 PEG chains/nm² corresponding to about 650 PEG chains per particle. DLS analysis of FA-PEG-GNP (Figure 3A) showed that upon PEG coating, the size of the particles increased from 14.6 ± 2.3 nm to 28.1 ± 5.2 nm. Notably, TEM imaging displayed a homogeneous coating corona surrounding the particles (Figure 3B) which was not present on the uncoated particles. UV-Vis spectroscopic analysis showed that the polymer coating resulted in a red shift of the maximum absorption from

520 nm to 523 nm (Figure 3C), which was attributed to the change in GNP surface features upon the replacement of the citrate corona with the polymers [33, 34].

Cell uptake of folate-targeted gold nanoparticles

The cell targeting capacity of gold nanoparticles was investigated using three human cell lines that were selected for their different expression of folate receptor (FR): KB and HCT-116 cells over-express FR, whereas MCF7 cells do not over-express FR [35]. A preliminary flow cytometric assay (Figure 4) confirmed that MCF7 cells did not over-express FR (integrated mean fluorescence intensity, iMFI 0.72 ± 0.51), whereas HCT-116 and KB cells over-expressed FR at low (iMFI 16.84 ± 1.20 , loFR) and high (iMFI 3309.04 ± 95.87 , hiFR) density, respectively. MCF7 cells were thus selected as negative control.

A quantitative FA-PEG-GNP and mPEG-GNP up-take by the three cell lines either in the presence or absence of free FA was obtained using atomic absorption spectrometry (Figure 5).

Under the selected incubation conditions [36], about 19800 and 2300 FA-PEG-GNP were found per KB cell and HCT-116 cell, respectively, which corresponded to the different FR expression of the two cell lines. On the contrary, non-targeted particles (mPEG-GNP) showed a 36 times lower association with KB cells and 22 times lower association with HCT-116 cells compared to the targeted ones. The MCF7 cell uptake of the targeted particles was very low (570 particles per cell).

The cell competition assay performed by cell co-incubation with FA-PEG-GNP and free folic acid showed significant folate targeted GNP internalization inhibition in both KB and HCT-116 cells.

TEM images of KB cells incubated with FA-PEG-GNP showed that the particles were endocytosised by the cells and confined into intracellular vesicles that originate from the plasma membrane (Figure 6A and B). Notably, particles do neither undergo aggregation throughout the endocytic process nor clustering. Control non-targeted particles incubated with KB cells were not massively taken up by the cells (Figure 6C and D). However, in all cases, few particles were barely detectable in the cytosol in all the cell lines.

Effects of folate-targeted gold nanoparticles on cell proliferation upon US treatment

The efficacy and selectiveness of FA-PEG-GNP as sonosensitizers was investigated by evaluating their sonodynamic activity on MCF7, HCT-116 and KB cell lines (Figure 7).

Cell exposure to US alone, (US_n and US_t), did not affect the MCF7, HCT-116 and KB cell growth (Figure 7A-C). Similarly, no effect on cell growth was observed when cells were treated with both non-targeted (mPEG-GNP, data not shown) and targeted (FA-PEG-GNP) nanoparticles alone, without US exposure (Figure 7A-C). Combined FA-PEG-GNP/ US treatment, with both US_n and US_t , led to significant decrease in HCT-116 and KB cell growth (Figure 7B-C). This did not occur in MCF7 cells (Figure 7A). Significant differences in the cytotoxicity were found when the loFR cells (HCT-116) incubated with FA-PEG-GNP were exposed to the two different US energy densities (US_n and US_t), with the US_t being the more efficient. Combined FA-PEG-GNP/ US treatment induced significant decreases in cell growth of $30.18 \pm 6.02\%$, $39.17 \pm 5.81\%$ and $55.65 \pm 9.80\%$ with US_n and $46.67 \pm 5.03\%$, 69.35 ± 8.74 and 82.04 ± 8.03 with US_t at 24, 48, 72 h, respectively as compared to untreated cells (Figure 7B). On the contrary, US_n and US_t gave the same decrease in cancer cell growth at each time point in hiFR cells (KB) treated with FA-PEG-GNP (Figure 7C), i.e. $68.8 \pm 7.09\%$, $78.29 \pm 8.96\%$ and $79.54 \pm 8.37\%$ with US_n and $67.77 \pm 8.04\%$, $86.48 \pm 9.15\%$ and $92.63 \pm 7.84\%$ with US_t at 24, 48 and 72 h, respectively as compared to untreated cells (Figure 7C).

To further confirm the selective sonosensitizing activity of the FA-PEG-GNP under US exposure, a competition assay was performed by cell co-incubation with FA-PEG-GNP and free FA (200 μ M) followed by US exposure. Notably, the cytotoxic activity of the sonodynamic treatment was completely suppressed both in HCT-116 (Figure 7D) and KB cells (Figure 7E).

Cell death study

The cell death mechanisms of HCT-116 and KB cells treated with FA-PEG-GNP/ US were investigated by a flow cytometric assay. Since the percentages of apoptotic and necrotic cells at 2, 6 and 12 h do not show any significant differences, we herein report only the cell death analysis at 2 h after FA-PEG-GNP/ US treatment to highlight the quick onset of cancer cell death (Figure 8). Cell death of HCT-116 and KB cells sonodynamically treated was found to occur with a significant increase ($p < 0.001$) in the percentages of late apoptotic/necrotic cells (Figure 8A, B). Furthermore, the FA-PEG-GNP sonoactivation with US_t induced a higher increase ($p < 0.01$) in the percentages of early apoptotic cells in KB (Figure 8B) as compared to HCT-116 cells (Figure 8A).

Intracellular ROS assessment upon folate-targeted gold nanoparticles incubation and US exposure

Since the mechanism underlying chemical sensitizer cytotoxicity upon US exposure is thought to be ROS generation [9], it was decided to evaluate ROS production after each treatment type. Cell incubation with FA-PEG-GNP without US activation did not induce an intracellular increase in ROS production in either cell line HCT-116 or KB (Figure 9). Cell exposure to US alone, in absence of FA-PEG-GNP, induced a very limited increase in ROS production at both US energy densities (Figure 9). The sonodynamic treatment of cells incubated with FA-PEG-GNP at both energy densities induced a significant increase in ROS production (Figure 9). The highest level of intracellular ROS was achieved 15 min after the exposure of HCT-116 cells to US_n (Figure 9A) and 1 min after the exposure of KB cells to US_t (Figure 9B). A less intense and delayed pattern of ROS generation was found in the loFR HCT-116 cells (Figure 9A), and a more intense and faster ROS generation pattern was shown by the hiFR KB cells (Figure 9B).

A ROS scavenging assay with N-acetylcysteine (NAC) was carried out to clarify the correlation between intracellular ROS production and the cancer cell death induced by FA-PEG-GNP/ US treatment. Interestingly, NAC suppressed ROS production and cytotoxicity only when FA-PEG-

GNP treated HCT-116 cells were sonoactivated with the lower US energy density US (Figure 10A, C). When these cells were treated with the higher US energy density, a remarkable decrease of cancer cell growth, as compared to untreated cells, was only observed after 72 h ($43.73 \pm 8.2\%$, Figure 10A). This was accompanied by a slight but significant increase in ROS production 1 min after US exposure (Figure 5B). On the other hand, in KB cells NAC was not able to suppress either ROS generation or US-triggered FA-PEG-GNP cytotoxicity at either energy density (Figure 10B). Notably, the amount of ROS generated by the FA-PEG-GNP/ US_t treatment, which caused a moderate increase of the medium temperature, at 1 min (Figure 10D) was equivalent to levels detected in the absence of the ROS scavenging agent (Figure 9B).

DISCUSSION

Improvements in therapeutic activity and selectivity are the major goals in the development of any innovative anticancer treatment. Many approaches have been introduced to achieve these goals and most of them have been based on drug delivery [37, 38]. However, combined strategies have recently attracted increasing levels of interest [39-41]. Photodynamic therapy (PDT) has been approved for clinical therapy and is the most widely accepted procedure of the “bimodal” anticancer approaches currently available. PDT still suffers from major drawbacks that limit its application to topical therapy, i.e. actinic keratosis and basal cell carcinoma, despite the great interest and promising results [42]. SDT has therefore been proposed as an alternative to PDT as it has the potential to overcome its major limitations and also because it may well be able to open up novel frontiers in cancer treatment.

Despite SDT’s promising advantages, the poor reproducibility of treatment outcomes and inadequate correlation between *in vitro* and the *in vivo* results have hampered the development of this robust treatment protocol, slowing its translation to clinical practice [43]. The development of innovative sonosensitizers is therefore paramount if we are to overcome these drawbacks and boost the effect of US and while taking advantage of the combined effects of possible sonoluminescence emitted by US exposure.

According to this hypothesis, US sensitive nanoparticles were designed in order to achieve accumulation in solid tumors by passive mechanisms and be internalized into cancer cells by active mechanisms. Therefore, gold nanoparticles were sized to exploit the enhanced tumor permeability and retention (EPR) effect and surface decorated to achieve the active targeting of cancer cells and cell internalization. The combination of these features with focused US treatment can provide for enhanced spatially controlled sonosensitizing effects.

As a proof of concept, gold nanoparticles were decorated with folic acid (FA-PEG-GNP) to bestow selectivity for cancer cells that over-express the folate receptor. Folic acid was conjugated to the particle surface via a PEG spacer which guarantees the exposure and flexibility of the biological

ligand. This directly results in efficient receptor mediated uptake by folate receptor expressing cancer cells. The selection of the targeting agent density was based on our previous studies showing that an average of 50 folate units per particle yielded suitable folate receptor biorecognition and high cell uptake efficiency of targeted gold nanoparticles [36].

The surface saturation of the FA-PEG-SH decorated nanoparticles with mPEG-SH was pursued to endow the particles with stealth properties while ensuring exposure of the targeting agent at the tip of the 3.5 kDa FA-PEG-SH chains. mPEG was found to enhance the colloidal stability of the particles and inhibit GNP aggregation as observed by intracellular TEM imaging, whereas did not prevent the FR recognition. The targeted particles were in fact efficiently taken up by FR over-expressing cancer cells and limitately internalized by the control cell line (MCF7) which does not over-express the FR. Selective recognition and cell uptake was confirmed by competition study with free folic acid, in which particle uptake was inhibited in HCT-116 and KB cells. Furthermore, the extent of particle association to cells was affected by the cell expression level of the FR, being higher in hiFR KB cells and lower in loFR HCT-116 cells. To note that the non-targeted control gold nanoparticles (mPEG-GNP) were barely detected in the cytosol of all cell lines by intracellular TEM imaging, which is probably due to negligible mPEG-GNP diffusion across cell membranes in agreement with previous studies reported by Kanaras *et al.* [34].

The selective cytotoxicity of the combined FA-PEG-GNP/ US treatment has been demonstrated by using cells with different degree of FR expression and by competitive studies.

Cytotoxicity studies showed that the sonoactivation of FA-PEG-GNP was ineffective in the case of cells that did not over-express the FR, namely MCF7. On the contrary, FA-PEG-GNP provide significant cancer cell sensitization to US which in turn yields selective and remarkable cytotoxicity in FR over-expressing HCT-116 and KB cells. This cytotoxic effect was suppressed when free folic acid was co-incubated with FA-PEG-GNP, demonstrating that the targeted nanoparticle cell uptake is paramount to the overall efficacy of the treatment. Thus, we can conclude that the synergistic effect between targeted gold nanoparticles and US-induced acoustic cavitation occurs upon particle

endocytosis.

In the literature it is reported that the success of the folic acid-targeted therapeutic system normally relies on the level of FR over-expression for a given tumor; low FR over-expressing cancers were found to have limited response to folate-targeted therapies [17, 44]. Nevertheless, the cytotoxicity results obtained on MCF7, HCT-116 and KB cells demonstrate the high selectivity of FA-PEG-GNP/ US treatment for all FR over-expressing cells. It is worth to note that the US-activated FA-PEG-GNP efficiently induced significant cell death in cells with low and high levels of FR over-expression. This sonoactivation process would therefore seem to be effective on a wide range of cancers, which include low and high FR over-expressing cells. Interestingly, despite loFR cells (HCT-116) have a 8.6 times lower targeted GNP uptake with respect to hiFR cells (KB), their response to the combined treatment with US_n and US_t is not so different, and this may be due to a higher HCT-116 cell sensitivity to US-induced ROS. These results suggest that the cytotoxicity induced by the sonoactivation of FA-PEG-GNP therefore does not only depend on the degree of FR over-expression, but also on the intrinsic cell sensitivity to the treatment outcomes, namely ROS [45].

The studies undertaken to elucidate the mechanism of cancer cell death induced by FA-PEG-GNP/ US treatment showed that incubation with FA-PEG-GNP and exposure to US_n or US_t provoked a sudden occurrence of necrotic rather than apoptotic cell death. When looking at the intracellular ROS production of the two cell lines that over-express FR and the two energy density exposures, different behaviours were observed. The higher intracellular ROS generation detected in hiFR KB cells may be ascribed to the higher amount of particle uptake compared to loFR HCT-116 cells (Figure 5). In the case of KB cells, ROS production was not found to depend on US energy density. On the contrary, the rate and level of intracellular ROS production in the loFR cell line was more rapid and higher in level at the highest energy density (US_t). These results suggest, as expected, that ROS production depends on both intracellular particle density and US intensity. In the case of high FA-PEG-GNP cell uptake obtained with KB cells, the effect of US energy density is negligible,

while in the case of low FA-PEG-GNP cell uptake observed in HCT-116 cells the US energy density is critical to the cytotoxicity.

The ROS scavenger NAC was used in order to provide additional information about the involvement of ROS in cell death upon the sonodynamic activation of intracellular FA-PEG-GNP. Interestingly, the effect of NAC was found to depend on both cell line and US energy density. NAC prevented HCT-116 cell death, supporting the hypothesis that the cytotoxicity was mainly ascribable to the ROS production. This hypothesis was further confirmed by the results obtained with KB cells, which endocytosed high amounts of FA-PEG-GNP. In this case, in fact the NAC effect could not be observed when the sonoactivation was performed with the higher US intensity because, under this condition, the ROS production was very high. On the contrary, when sonoactivation was performed with the lower US intensity, that produced a not so high level of ROS, NAC efficiently suppressed intracellular ROS generation and cytotoxicity.

One mechanistic explanation of the effects that are induced upon GNP US-exposure is that ROS production might also be a consequence of the gold nanoparticle SPR effect. Accordingly, US-induced cavitation can generate light that is absorbed by GNP and quickly converted to heat which induces ROS production and cancer cell death. This hypothesis appears to be in line with observations made by Sazgarnia *et al.* [46]. Indeed, these authors investigated sonoluminescence on a gel phantom containing gold nanoparticles loaded with propoporphyrin IX. They highlighted the occurrence of gas bubbles, transient cavitation upon US irradiation, the collapse of the bubbles, sonoluminescence and free radical generation. Moreover, Wang *et al.* [47] developed a gold nanoparticle coated mesoporous silica nanocapsule-based platform that, under the guidance of intensified US imaging, was able to enhance HIFU ablation efficacy on rabbit xenograft tumors. Other metal nanoparticles, such as ZnONPs [48] and TiO₂NPs [48, 49], may also be suitable for use as sonosensitizers due to their inherent ability to absorb sonoluminescence irradiation. However, GNP show several beneficial properties, such as the ability to behave as localized thermal loaders

[50], while they also possess a non-toxic and biocompatible metal core [13, 51], making them an intriguing platform for the development of the next generation of nanosonosensitizers.

CONCLUSIONS

The ability of US to activate the targeted gold nanoparticles for cancer cell killing in FR over-expressing cell lines confirmed the hypotheses published by Wen *et al.* [52] that the combination of gold nanoparticles and US may be a promising strategy for future medical applications. To the best of our knowledge, our study demonstrates for the first time the role of targeted gold nanoparticles as sonosensitizers. Indeed, the results reported here concerning targeted gold nanoparticles for sonodynamic treatment showed a remarkable decrease in cancer cell growth at different US treatment conditions (US_n and US_t).

In conclusion, targeting GNP have proven themselves to be effective sonosensitizers for the US-based treatment of cancer paving the way to novel approach in selective cancer treatments.

FIGURE LEGENDS

Figure 1. MALDI-TOF spectrum of (A) NH₂-PEG-SH and (B) FA-PEG-SH conjugate.

Figure 2. (A) dynamic light scattering profile and (B) TEM image of naked gold nanoparticles.

Figure 3. (A) dynamic light scattering profile and (B) TEM image of FA-PEG-GNP. (C) UV-Vis spectrum of naked GNP (black line) and FA-PEG-GNP (red line) in deionized water.

Figure 4. Folate receptor expression of MCF7, HCT-116 and KB cells by flow cytometry. Data are expressed as integrated mean fluorescence intensity (iMFI), defined as the percentage of FR-positive cells multiplied by mean fluorescence intensity of FR-positive cells.

Figure 5. Cell uptake profile of folate targeted (FA-PEG-GNP) and non-targeted (mPEG-GNP) gold nanoparticles by MCF7, HCT-116 and KB cell lines. Folate targeted GNP were also incubated with cells in the presence of free folic acid (FA) as competitive agent. Statistical significance was calculated versus folate targeted particle uptake tested on each cell line: * $p < 0.05$, ** $p < 0.01$, *** $p < 0.001$.

Figure 6. (A, B) TEM images of KB cells incubated with folate targeted gold nanoparticles and (C, D) non-targeted gold nanoparticles. Red arrows indicate gold nanoparticles.

Figure 7. Effect of FA-PEG-GNP upon irradiation with US on cell lines with differing FR expression. Cells were exposed for 2 h to 1 nM FA-PEG-GNP and US irradiation was carried out for 5 min at two different energy densities (US_n: 0.008 mJ/cm² and US_t: 0.080 mJ/cm²). The upper panels show the effect of FA-PEG-GNP irradiated by US (both US_n and US_t), of US alone (both US_n and US_t) and of FA-PEG-GNP alone on MCF7 (A), HCT-116 (B) and KB (C) cell growth. The lower panels report the effect of FA-PEG-GNP irradiated by US (both US_n and US_t), of US alone (both US_n and US_t) and of FA-PEG-GNP alone on HCT-116 (D) and KB (E) cell growth with 200 μM free FA added to the culture medium to evaluate the receptor mediated uptake selectivity of FA-PEG-GNP. Statistically significant difference versus untreated cells: * $p < 0.05$; ** $p < 0.01$; *** $p < 0.001$ and between US_n and US_t treatment: # $p < 0.05$.

Figure 8. Cell death induced by FA-PEG-GNP irradiated with US. HCT-116 (A) and KB (B) cells were exposed for 2 h to 1 nM FA-PEG-GNP and US irradiation was carried out for 5 min at two different energy densities (US_n : 0.008 mJ/cm² and US_t : 0.080 mJ/cm²). Cells were stained with APC-Annexin V and Sytox[®] Green 2 h after the different treatment types and analysed by flow cytometry to quantify the viable cells (negative to APC-Annexin V and Sytox[®] Green), early apoptotic cells (positive to APC-Annexin V and negative to Sytox[®] Green), and late apoptotic/necrotic cells (positive to Annexin V and Sytox[®] Green). Statistically significant difference versus untreated cells: * $p < 0.05$; ** $p < 0.01$; *** $p < 0.001$.

Figure 9. ROS production induced by FA-PEG-GNP irradiation with US. HCT-116 (A) and KB (B) cells were exposed for 2 h to 1 nM FA-PEG-GNP and US exposure was carried out for 5 min at at two different energy densities (US_n : 0.008 mJ/cm² and US_t : 0.080 mJ/cm²). ROS production after the different treatment types was quantified according to the dichlorofluorescein-diacetate assay with flow cytometry and expressed as integrated mean fluorescence intensity (iMFI) ratio to yield the ratiometric increase in fluorescence per time point. Statistically significant difference versus untreated cells: * $p < 0.05$; ** $p < 0.01$; *** $p < 0.001$.

Figure 10. Effect of the reactive oxygen species (ROS) scavenging agent, N-acetylcysteine (NAC), on cell proliferation and ROS production as induced by FA-PEG-GNP's irradiation with US. HCT-116 (A, C) and KB (B, D) cells were exposed for 2 h to 1 nM FA-PEG-GNP with the addition of 5.0 mM NAC to the culture medium and US exposure was carried out for 5 min at two different energy densities (US_n : 0.008 mJ/cm² and US_t : 0.080 mJ/cm²). The left panels (A, B) report the effect of FA-PEG-GNP irradiation with US (both US_n and US_t), of US alone (both US_n and US_t) and of FA-PEG-GNP alone in the presence of the ROS scavenging agent, NAC. The right panels (C, D) report the ROS production of FA-PEG-GNP irradiated with US (both US_n and US_t), of US alone (both US_n and US_t) and of FA-PEG-GNP alone in the presence of the ROS scavenging agent, NAC. Statistically significant difference versus untreated cells: * $p < 0.05$; ** $p < 0.01$; *** $p < 0.001$.

SUMMARY POINTS

- Folate-PEG decorated gold nanoparticles (FA-PEG-GNP) have been designed to target folate receptor over-expressing human cancer cells.
- The gold nanoparticles were generated by reduction of chloroauric acid and coated with a folate-PEG-SH (FA-PEG-SH) at a density of 50 FA-PEG-SH units per particle and then surface saturated with methoxy-PEG-SH (mPEG-SH).
- *In vitro* experiments performed on folate receptor over-expressing (KB and HCT-116) and non over-expressing (MCF7) human cancer cells showed that the particle association to the cells correlated to the folate receptor expression.
- Competition cell up-take assays performed in the presence of folic acid confirmed that FA-PEG-GNP selectively targeted KB and HCT-116 cells.
- A selective killing of cancer cells with a peculiar signature (namely over-expression of a selected receptor) was achieved by cancer cell incubation with targeted gold nanoparticles and exposure to two different ultrasound energy densities.
- The combined approach of targeted gold nanoparticles and ultrasound exposure was able to determine a remarkable reactive oxygen species (ROS) generation and increase in necrotic cancer cells, compared to control conditions.
- When KB and HCT-116 cells were treated with FA-PEG-GNP at the lower US energy density, N-acetylcysteine, used as ROS scavenger, completely suppressed ROS production and cytotoxicity.
- This is the first work that demonstrates how cancer targeted GNP can act as ultrasound sensitizers by themselves paving the way to a promising strategy for the site-specific treatment of cancer.

ACKNOWLEDGEMENTS

Authors would like to thank Prof. Ravi Kumar for inspiring their collaboration and Dr. Dale Lawson for his critical proof reading and advice.

FINANCIAL & COMPETING INTERESTS DISCLOSURE

This work was financially supported by Associazione Italiana per la Ricerca sul Cancro (grant “MFAG 2012,” MFAG-13048), by University of Torino (grant “Ricerca Locale 2015”) and by University of Padova (grant “Progetto di Ricerca di Ateneo” CPDA121714, CUP C94H12000020005 and grant “Progetto strategico di ateneo - Bando 2011” C98C13002740005, PROT. STPD11RYPT_02). The authors have no other relevant affiliations or financial involvement with any organization or entity with a financial interest in or financial conflict with the subject matter or materials discussed in the manuscript apart from those disclosed. No writing assistance was utilized in the production of this manuscript.

REFERENCES

1. Frenkel V. Ultrasound mediated delivery of drugs and genes to solid tumors. *Adv Drug Deliv Rev* 60(10), 1193-1208 (2008).
2. Leighton TG. What is ultrasound? *Prog Biophys Mol Biol* 93(1-3), 3-83 (2007).
3. Kennedy JE. High-intensity focused ultrasound in the treatment of solid tumours. *Nat Rev Cancer* 5(4), 321-327 (2005).
4. Mchale AP, Callan JF, Nomikou N, Fowley C, Callan B. Sonodynamic Therapy: Concept, Mechanism and Application to Cancer Treatment. *Adv Exp Med Biol* 880 429-450 (2016).
5. Suslick KS, Flannigan DJ. Inside a collapsing bubble: sonoluminescence and the conditions during cavitation. *Annu Rev Phys Chem* 59 659-683 (2008).
6. Vazquez G, Camara C, Putterman S, Weninger K. Sonoluminescence: nature's smallest blackbody. *Opt Lett* 26(9), 575-577 (2001).
7. Tachibana K, Feril LB, Jr., Ikeda-Dantsuji Y. Sonodynamic therapy. *Ultrasonics* 48(4), 253-259 (2008).
8. Umemura S, Yumita N, Nishigaki R, Umemura K. Mechanism of cell damage by ultrasound in combination with hematoporphyrin. *Jpn J Cancer Res* 81(9), 962-966 (1990).
9. Misik V, Riesz P. Free radical intermediates in sonodynamic therapy. *Ann N Y Acad Sci* 899 335-348 (2000).
10. Dolmans DE, Fukumura D, Jain RK. Photodynamic therapy for cancer. *Nat Rev Cancer* 3(5), 380-387 (2003).
11. Libutti SK, Paciotti GF, Byrnes AA *et al.* Phase I and pharmacokinetic studies of CYT-6091, a novel PEGylated colloidal gold-rhTNF nanomedicine. *Clin Cancer Res* 16(24), 6139-6149 (2010).
12. Kim BY, Rutka JT, Chan WC. Nanomedicine. *N Engl J Med* 363(25), 2434-2443 (2010).
13. Khlebtsov N, Dykman L. Biodistribution and toxicity of engineered gold nanoparticles: a review of in vitro and in vivo studies. *Chem Soc Rev* 40(3), 1647-1671 (2011).

14. Huang X E-SM. Gold nanoparticles: optical properties and implementations in cancer diagnosis and photothermal therapy. *Journal of Advanced Research* 1 13-28 (2010).
15. Link S E-SM. Shape and size dependence of radiative, non-radiative and photothermal properties of gold nanocrystals. *Int Rev Phys Chem* 19(3), 409-453 (2000).
16. Kennedy LC, Bickford LR, Lewinski NA *et al.* A new era for cancer treatment: gold-nanoparticle-mediated thermal therapies. *Small* 7(2), 169-183 (2011).
17. Bazak R, Hourri M, El Achy S, Kamel S, Refaat T. Cancer active targeting by nanoparticles: a comprehensive review of literature. *J Cancer Res Clin Oncol* 141(5), 769-784 (2015).
18. Mehra NK, Mishra V, Jain NK. Receptor-based targeting of therapeutics. *Ther Deliv* 4(3), 369-394 (2013).
19. Feng D, Song Y, Shi W, Li X, Ma H. Distinguishing folate-receptor-positive cells from folate-receptor-negative cells using a fluorescence off-on nanoprobe. *Anal Chem* 85(13), 6530-6535 (2013).
20. Krystofiak Es MV, Steeber Da, Oliver Ja. Elimination of Tumor Cells Using Folate Receptor Targeting by Antibody-Conjugated, Gold-Coated Magnetite Nanoparticles in a Murine Breast Cancer Model. *Journal of Nanomaterials* 2012 1-9 (2012).
21. Sims GE, Snape TJ. A method for the estimation of polyethylene glycol in plasma protein fractions. *Anal Biochem* 107(1), 60-63 (1980).
22. Kranz DM, Patrick TA, Brigle KE, Spinella MJ, Roy EJ. Conjugates of folate and anti-T-cell-receptor antibodies specifically target folate-receptor-positive tumor cells for lysis. *Proc Natl Acad Sci U S A* 92(20), 9057-9061 (1995).
23. Riddles PW, Blakeley RL, Zerner B. Ellman's reagent: 5,5'-dithiobis(2-nitrobenzoic acid)--a reexamination. *Anal Biochem* 94(1), 75-81 (1979).
24. Turkevich P SP, Hillier J. The formation of colloidal gold. *The journal of Physical Chemistry* 57(7), 670-673 (1953).

25. Liu X, Atwater M, Wang J, Huo Q. Extinction coefficient of gold nanoparticles with different sizes and different capping ligands. *Colloids Surf B Biointerfaces* 58(1), 3-7 (2007).
26. Jain Pk LK, El-Sayed Ih, El-Sayed Ma. Calculated absorption and scattering properties of gold nanoparticles of different size, shape, and composition: applications in biological imaging and biomedicine. *The Journal of Physical Chemistry B* 110(14), 7238-7248 (2006).
27. Link S E-SM. Spectral properties and relaxation dynamics of surface plasmonic oscillations in gold and silver nanodots and nonorods. *The Journal of Physical Chemistry B* 103(40), 8410-8426 (1999).
28. Gallon E, Matini T, Sasso L *et al.* Triblock Copolymer Nanovesicles for pH-Responsive Targeted Delivery and Controlled Release of siRNA to Cancer Cells. *Biomacromolecules* 16(7), 1924-1937 (2015).
29. Durando G GC, Canaparo R, Serpe L. Acoustic characterization of ultrasound fields able to induce sonodynamic activity in an in vitro cancer model. *2015 IEEE International Symposium on Medical Measurements and Applications, MeMeA 2015 - Proceedings* 121-124 (2015).
30. Matini T FN, Battocchio a, Spain Sg, Mantovani G, Vicent Mj, Sanchis J, Gallon E, Mastrotto F, Salmaso S, Caliceti P, Alexander C. Synthesis and characterization of variable conformation pH responsive block copolymers for nucleic acid delivery and targeted cell entry. *Polymer Chemistry* 5(5), 1626-1636 (2014).
31. Turkevich P SP, Hillier J. A study of the nucleation and growth processes in the synthesis of colloidal gold. *Discussions of the Faraday Society* 11 55-75 (1951).
32. Dreaden EC, Austin LA, Mackey MA, El-Sayed MA. Size matters: gold nanoparticles in targeted cancer drug delivery. *Ther Deliv* 3(4), 457-478 (2012).

33. Chuang Mk CF, Hsu Cs. Gold Nanoparticle-Graphene Oxide Nanocomposites That Enhance the Device Performance of Polymer Solar Cells. *Journals of Nanomaterials* 12 (2014).
34. Kanaras AG, Kamounah FS, Schaumburg K, Kiely CJ, Brust M. Thioalkylated tetraethylene glycol: a new ligand for water soluble monolayer protected gold clusters. *Chem Commun (Camb)* (20), 2294-2295 (2002).
35. Chen H, Ahn R, Van Den Bossche J, Thompson DH, O'halloran TV. Folate-mediated intracellular drug delivery increases the anticancer efficacy of nanoparticulate formulation of arsenic trioxide. *Mol Cancer Ther* 8(7), 1955-1963 (2009).
36. Mastrotto F, Caliceti P, Amendola V *et al.* Polymer control of ligand display on gold nanoparticles for multimodal switchable cell targeting. *Chem Commun (Camb)* 47(35), 9846-9848 (2011).
37. Swain S, Babu SM, Beg S, Jena J. Nanoparticles for Cancer Targeting: Current and Future Directions. *Curr Drug Deliv* (2016).
38. Xu X, Ho W, Zhang X, Bertrand N, Farokhzad O. Cancer nanomedicine: from targeted delivery to combination therapy. *Trends Mol Med* 21(4), 223-232 (2015).
39. Obaid G, Broekgaarden M, Bulin AL *et al.* Photonanomedicine: a convergence of photodynamic therapy and nanotechnology. *Nanoscale* 8(25), 12471-12503 (2016).
40. Qian X, Zheng Y, Chen Y. Micro/Nanoparticle-Augmented Sonodynamic Therapy (SDT): Breaking the Depth Shallow of Photoactivation. *Adv Mater* doi:10.1002/adma.201602012 (2016).
41. Serpe L FF, Canaparo R. Nanosonotechnology: the next challenge in cancer sonodynamic therapy. *Nanotechnology Reviews* 1(2), 173-182 (2012).
42. Agostinis P, Berg K, Cengel KA *et al.* Photodynamic therapy of cancer: an update. *CA Cancer J Clin* 61(4), 250-281 (2011).

43. Costley D, Mc Ewan C, Fowley C *et al.* Treating cancer with sonodynamic therapy: a review. *Int J Hyperthermia* 31(2), 107-117 (2015).
44. Serpe L GM, Canaparo R, Dosio F. Targeted treatment of folate receptor-positive platinum-resistant ovarian cancer and companion diagnostics, with specific focus on vintafolide and etarfolatide. *Pharmacogenomics Pers Med* 7 31-42 (2014).
45. Trachootham D, Alexandre J, Huang P. Targeting cancer cells by ROS-mediated mechanisms: a radical therapeutic approach? *Nat Rev Drug Discov* 8(7), 579-591 (2009).
46. Sazgarnia A, Shanei A, Eshghi H, Hassanzadeh-Khayyat M, Esmaily H, Shanei MM. Detection of sonoluminescence signals in a gel phantom in the presence of Protoporphyrin IX conjugated to gold nanoparticles. *Ultrasonics* 53(1), 29-35 (2013).
47. Wang X, Chen H, Zheng Y *et al.* Au-nanoparticle coated mesoporous silica nanocapsule-based multifunctional platform for ultrasound mediated imaging, cytolysis and tumor ablation. *Biomaterials* 34(8), 2057-2068 (2013).
48. Harada Y, Ogawa K, Irie Y *et al.* Ultrasound activation of TiO₂ in melanoma tumors. *J Control Release* 149(2), 190-195 (2011).
49. You DG, Deepagan VG, Um W *et al.* ROS-generating TiO₂ nanoparticles for non-invasive sonodynamic therapy of cancer. *Sci Rep* 6 23200 (2016).
50. Chirico G, Pallavicini P, Collini M. Gold nanostars for superficial diseases: a promising tool for localized hyperthermia? *Nanomedicine (Lond)* 9(1), 1-3 (2014).
51. Yildirimer L, Thanh NT, Loizidou M, Seifalian AM. Toxicology and clinical potential of nanoparticles. *Nano Today* 6(6), 585-607 (2011).
52. D W. Nanoparticle-Related Heat Transfer Phenomenon and Its Application in Biomedical Fields. *Heat Transfer Engineering* 34(14), 1171-1179 (2013).